Biomaterials Science

PAPER

View Article Online
View Journal | View Issue

Cite this: *Biomater. Sci.*, 2019, **7**, 3906

Carbon nanotube doped pericardial matrix derived electroconductive biohybrid hydrogel for cardiac tissue engineering†

Kaveh Roshanbinfar, [a,b,c] Zahra Mohammadi,*[c] Abdorreza Sheikh-Mahdi Mesgar,[c] Mohammad Mehdi Dehghan,[d] Oommen P. Oommen, [e] Jöns Hilborn*[f] and Felix B. Engel *[a,b]

Cardiovascular diseases represent a major socio-economic burden. In recent years, considerable effort has been invested in optimizing cell delivery strategies to advance cell transplantation therapies to restore heart function for example after an infarct. A particular issue is that the implantation of cells using a non-electroconductive matrix potentially causes arrhythmia. Here, we demonstrate that our hydrazide-functionalized nanotubes-pericardial matrix-derived electroconductive biohybrid hydrogel provides a suitable environment for maturation of human-induced pluripotent stem cell (hiPSC)-derived cardiomyocytes. hiPSC-derived cardiomyocytes exhibited an improved contraction amplitude (>500%) on conductive hydrogels compared to cells cultured on Matrigel®. This was accompanied by increased cellular alignment, enhanced connexin 43 expression, and improved sarcomere organization suggesting maturation of the hiPSC-derived cardiomyocytes. Sarcomeric length of these cells increased from 1.3 to 1.7 μm. Moreover, 3D cell-laden engineered tissues exhibited enhanced calcium handling as well as positive response to external electrical and pharmaceutical stimulation. Collectively, our data indicate that our biohybrid hydrogels consisting of solubilized nanostructured pericardial matrix and electroconductive positively charged hydrazide-conjugated carbon nanotubes provide a promising material for stem cell-based cardiac tissue engineering.

Received 18th March 2019,
Accepted 9th July 2019

DOI: 10.1039/c9bm00434c

rsc.li/biomaterials-science

Introduction

The major cause of heart failure in most cases is the loss of cardiomyocytes as humans have no or at best a limited ability to generate new cardiomyocytes.[1] This leads to progressive scar formation, ventricular wall dilatation, secondary loss of cardiomyocytes, and eventually heart failure. Even though great advances have been achieved in identifying risk factors and to reduce damage by immediate measurements, for example by acute percutaneous coronary intervention, the prevalence of heart failure is increasing.[2,3] As a result of public health and medicine, the mortality of coronary artery diseases declined since the 1960s by ~40%;[4] however, the quality of life for those patients who survived from an infarct is still undermined by hospitalization and long waiting lists for receiving appropriate transplantations.[2] Therefore, major effort is invested to develop therapies to prevent, reduce, and reverse damage to the heart. Currently, the only available therapy is heart transplantation, which is severely limited due to a shortage of donor organs.[5,6]

In order to reverse cardiomyocyte loss efforts have been devoted to adding cardiomyocytes or by enhancing the

[a]*Experimental Renal and Cardiovascular Research, Department of Nephropathology, Institute of Pathology, Friedrich-Alexander-Universität Erlangen-Nürnberg (FAU), 91054 Erlangen, Germany. E-mail: felix.engel@uk-erlangen.de; Fax: +49 9131 85 25699; Tel: +49 9131 85 25699*

[b]*Muscle Research Center Erlangen (MURCE), 91054 Erlangen, Germany*

[c]*Biomaterials group, Bioceramics laboratory, Biomedical Engineering Department, Faculty of New Sciences and Technologies, University of Tehran, 1439957131 Tehran, Iran*

[d]*Department of Surgery and Radiology, Faculty of Veterinary Medicine, University of Tehran, Tehran, 1417466191, Iran*

[e]*Bioengineering and Nanomedicine Lab, Faculty of Biomedical Sciences and Engineering, Tampere University of Technology and BioMediTech Institute, 33720 Tampere, Finland*

[f]*Department of Chemistry, Angstrom Laboratory, Uppsala University, SE 75121 Uppsala, Sweden*

†Electronic supplementary information (ESI) available: Fig. S1 (showing proliferation and differentiation of hMSCs as well as viability of hiPSC-derived cardiomyocytes after 24 h on different substrates), Movie S1 (hiPSC-derived cardiomyocytes on Matrigel® at day 7), Movie S2 (hiPSC-derived cardiomyocytes on PM at day 7), Movie S3 (hiPSC-derived cardiomyocytes on PMCNT at day 7), Movie S4 (Calcium handling of PM-tissues at day 7), and Movie S5 (Calcium handling of PMCNT-tissues at day 7), Movie S6 (PM-tissues at day 27), and Movie S7 (PMCNT-tissues at day 27). See DOI: 10.1039/c9bm00434c

endogenous regenerative potential of the heart.[1] In terms of adding cardiomyocytes, a large effort is invested in promoting differentiation and maturation of human embryonic stem cells (hESC) or human induced pluripotent stem cells (hiPSC) in adult-like cardiomyocytes and in determining the best strategy to implant these cells into the injured heart.[7] Major existing issues are maturation of hESC- and hiPSC-derived cardiomyocytes and induction of arrhythmia.[8–10] In terms of promoting the endogenous regenerative potential of the heart, it remains unclear whether it can indeed be enhanced to significantly improve heart function. Yet, clinical trials have at least verified that transplanted stem cells such as human mesenchymal stromal cells (hMSCs) improve heart function in a paracrine fashion.[1,11] In addition, it has recently proposed that the beneficial effects observed in animal models upon implantation of hiPSC-derived cardiomyocytes are the result of a paracrine effect and probably not due to the contractile force of the cells.[12,13] The underlying mechanism of the paracrine effect, however, remains unclear. It is possible that secreted factors/extracellular vesicles (EVs) promote cardiomyocyte proliferation or proliferation and cardiac differentiation of endogenous stem cells. A current debate is whether cell transplantation is necessary or the application of factors/EVs is sufficient.[14–16] Yet, it is clear that so far cell-free as well as cell-based strategies are not advanced enough to decide which of both will be successful in the future.

The clinical outcome of cell-based therapy remains unsatisfactory but the so far obtained results are promising and encourage continuing to better understand and optimize this strategy. Major obstacles are the low engraftment and limited survival rate of transplanted cells in the injured host tissue.[17,18] In addition, the transplanted cells and materials will act as a non-conductive scar enhancing the risk of arrhythmia.[19] Therefore, new materials are needed that are electroconductive and allow stem cells to proliferate, which will increase the amount of secreted factors/EVs, and/or to promote maturation of hiPSC-derived cardiomyocytes. Several approaches are known to enhance conductivity such as the addition of electroconductive materials including nanoparticles,[20] nanorods,[21] nanowires,[22] carbon nanotubes,[23,24] or conductive polymers.[25,26] In the field of cardiac tissue engineering polyaniline (PANi)[27] and polypyrrole (PPy)[28–30] are the most utilized materials to enhance electrical conductivity. While it has been shown that PANi and PPy are promising, they have the major disadvantage of not being dispersible in water.[31,32] Thus, they cannot be used together with cells during the production steps. Therefore, there is an urgent need for electroconductive materials, which are dispersible in water and compatible with cells suitable to promote cardiac repair. Currently, there is to our knowledge only one such polymer, electroconductive poly(3,4-ethylenedioxythiophene) : polystyrene sulfonate (PEDOT : PSS), in the literature described.[33] The suitability of PEDOT : PSS combined with alginate and collagen has been tested in the context of hiPSC-derived cardiomyocytes. However, due to its intrinsically low mechanical properties, this material could not enhance the mechanical properties of the biohybrid hydrogel. This would represent a limitation in tunability of mechanical properties of the final hydrogel. Metallic nanoparticles are another group of conductive materials, which have been used for tissue engineering applications. However, their use in hydrogels might result in inhomogeneous mechanical properties and thereby forming points of stress concentrations, which can alter the outcome of the final product.[34] Carbon nanotubes are promising due to their morphology as well as anisotropic mechanical and electrical properties. However, a possible problem, especially with multi-walled carbon nanotubes, is to obtain a stable solution.[35] Thus, we previously developed stably dispersed nanotubes in water that can be used together with gels.[23] These positively charged nanotubes could theoretically interact with the negatively charged cellular membrane of cardiomyocytes and enhance their function by improving cellular attachment. Here, we tested our electroconductive biohybrid hydrogel consisting of nanofibrous decellularized pericardial matrix from young adult sheep heart and the above described electroconductive, positively charged hydrazide-conjugated multiwall carbon nanotubes[23] in the context of hMSC as well as hiPSC-derived cardiomyocytes in order to expand the opportunities to deliver stem cells and/or produce electroconductive cardiac tissues. While a variety of different biomaterials have been evaluated for cardiac tissue engineering,[36,37] decellularized matrices are promising as they conserve different elements from native extracellular matrix (ECM).[38] Maintaining the ECM complexity, these materials provide the cells with mechanical integrity and participate in signaling events that play an important role in cell fate.[38,39] However, these materials are mechanically weak and they are not electrically conductive. These limiting factors may hamper their efficiency when used for regenerating electroactive cardiac tissue. Thus, we utilized carbon nanotubes, which due to their unique characteristics improved mechanical and electrical properties of the hydrogels.[40–42]

Here we aimed at determining whether our hydrogel provides a proper microenvironment to enhance mesenchymal stromal cell proliferation as well as cardiomyocyte maturation. Our data indicate that our biohybrid hydrogel provides a promising material for stem cell-based cardiac tissue engineering. It promotes proliferation of hMSCs as well as maturation of hiPSC-derived cardiomyocytes evidenced by improved contraction amplitude in agreement with increased alignment, enhanced connexin 43 expression, improved sarcomere organization, and increased sarcomeric length.

Results

Preparation and characterization of pericardial matrix-derived electroconductive biohybrid hydrogel

As described previously,[23] we have functionalized multiwall carbon nanotubes (MWCNT-COOH) with carbodihydrazide (CDH) using *N*-(3-dimethylaminopropyl)-*N*′-ethylcarbodiimide coupling reaction to obtain hydrazide-functionalized nano-

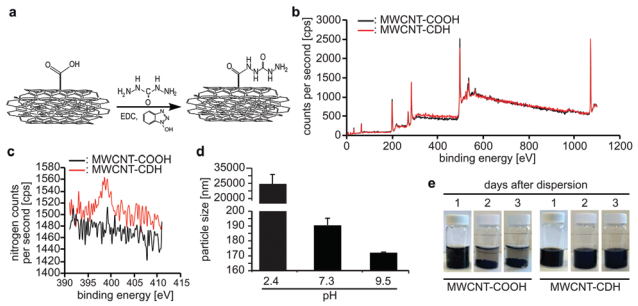

Fig. 1 Preparation of nanotubes and hydrogels. (a) Schematic illustration of substituting carboxylic acid functional groups on the MWCNTs with positively charged hydrazide functional groups. (b) Representative elemental analyses by X-ray photoelectron spectroscopy(XPS). (c) XPS-analysis of nanotubes for nitrogen atoms at N 1s binding energy intensity. (d) Analyses of particle size for MWCNT-CDH at different pH values. (e) Representative photograph images of MWCNT-COOH and MWCNT-CDH to study the stability of the water-dispersed nanotubes.

tubes (MWCNT-CDH) (Fig. 1a). Analysis of the nanotubes using X-ray photoelectron spectroscopy (XPS) before and after modification verified the successful conjugation of hydrazide functional groups at 4 mol%. This has been calculated by the internal software of the machine based on the NIST X-ray Photoelectron Spectroscopy Database (Fig. 1b and c) and indicates the presence of $-NHNH_2$ functional groups.

Dynamic light scattering measurements revealed that MWCNT-CDH in water formed particles with a diameter of ~190 nm at physiological pH (Fig. 1d). Lower pH values resulted in a significant increase in particle size (~25 μm at pH 2.4) while particle size further decreased by increasing pH-values (~170 nm at pH 9.5). In order to evaluate time-dependent stability of modified nanotubes, stationary vials filled with nanotubes dispersed in water at physiological pH were monitored for 3 days. In contrast to MWCNT-COOH, MWCNT-CDHs were stable upon dispersion even after 3 days (Fig. 1e).

Next, we prepared a new batch of decellularized solubilized pericardial matrix following the previously reported protocol (Fig. 2a).[23] For this purpose, we obtained adult sheep pericardium, rinsed and cleaned it thoroughly from blood and adipose tissue, decellularized and enzymatically digested the remaining tissue. Decellularization was verified based on hematoxylin and eosin staining (Fig. 2b) and quantification of genetic material by measuring DAPI intensity (Fig. 2c). Sulphated glycosaminoglycan (sGAG) content of the decellularized solubilized matrix was measured by dimethyl-methylene blue (DMMB) assay and compared to the fresh tissue (Fig. 2d). Our data show that decellularization significantly decreased sGAG content. However, molecular weight analysis of protein content of decellularized tissues by polyacrylamide gel electrophoresis (PAGE) indicates that proteins with a molecular weight comparable to collagen have been preserved compared to fresh tissue (Fig. 2e). Finally, we mixed the solubilized matrix with MWCNT-CDH in order to form a biohybrid pre-gel and incubation at 37 °C for 30 min resulted in the formation of a

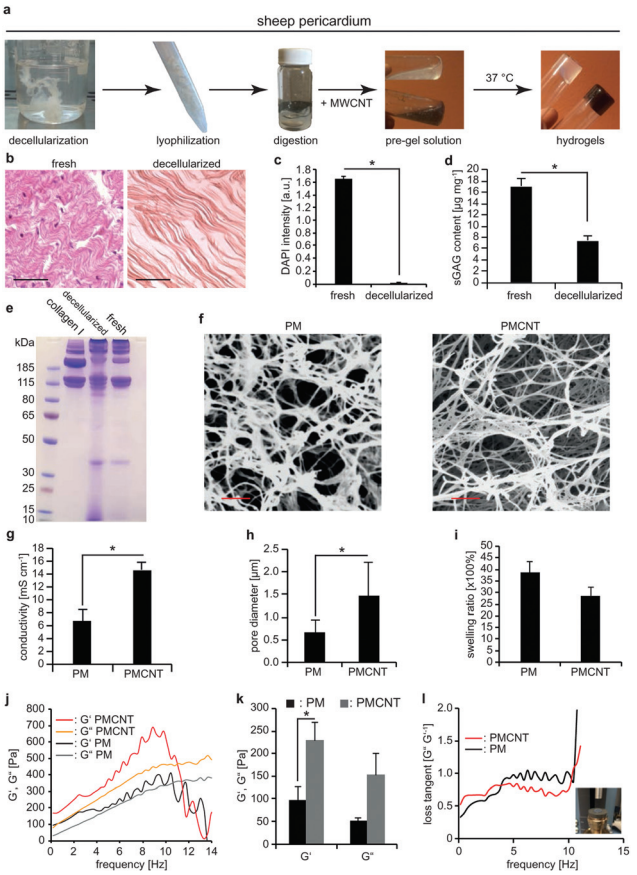

Fig. 2 Material properties of conductive biohybrid hydrogels. (a) Illustration of different steps in preparation of PM- and PMCNT-gels. (b) Representative histological images of fresh and decellularized pericardium based on hematoxylin–eosin staining. Blue points represent cellular nuclei. (c) Quantitative analyses of DNA content in fresh and decellularized pericardium. (d) Quantitative analyses of sGAG content by DMMB assay. (e) Analysis of molecular weight of the protein content by PAGE measured from 35 μg total protein loaded in each well. (f) Representative SEM images of PM- and PMCNT-gels. (g) Quantitative analyses of electrical conductivity measured by four-point-probe test. (h) Quantitative analyses of pore diameter based on SEM images. (i) Quantitative analyses of swelling ratio of PM- and PMCNT-gels. (j) Analyses of quantitative changes in storage and loss modulus as a function of frequency. (k) Quantitative analyses of shear storage (G') and loss modulus (G'') measured from rheological analyses. (l) Quantitative analyses of loss tangent as an indication of dampening properties of the gels as a function of frequency. Data are mean ± SD. *: $p < 0.05$ and for all quantified data $n = 3$. Scale bars: black: 50 μm, red: 1 μm.

stable gel (from now on termed as PMCNT-gel). Four-point-probe measurements confirmed that the addition of MWCNT-CDH increased the conductivity of pericardial matrix hydrogel (from now on termed as PM-gel) from 6.7 ± 1.8 mS cm^{-1} to 14.6 ± 1.2 mS cm^{-1} for pericardial matrix hydrogel containing MWCNT-CDH (Fig. 2g).

As previously shown,[23] PM- and PMCNT-gels exhibit an ECM-like nanofibrous structure (Fig. 2f). Analysis of scanning electron microscopy (SEM) images of critically point dried samples after sputter-coating by gold revealed that incorporation of MWCNT-CDH resulted in increased pore diameter

from 0.6 ± 0.3 μm for PM-gels to 1.5 ± 0.7 μm for PMCNT-gels (Fig. 2h). The swelling ratio was not significantly affected by the presence of MWCNT-CDH (Fig. 2i) while the storage modulus (G') was significantly increased (Fig. 2j and k). Finally, we calculated the ratio of G'' to G', which is known as loss tangent ($\tan(\delta) = G''G'^{-1}$). It provides a measure of dampening of the material. In the range of physiological cardiac frequencies, loss tangent for PMCNT-gels was 0.42 ± 0.002 while it was 0.77 ± 0.007 for PM-gels. This shows that PMCNT-gels are more elastic than PM-gels storing more energy while stressed and exhibiting lower energy damping (Fig. 2l).

PMCNT-gels are suitable materials for cardiac therapy relevant cell types

Previously, we have demonstrated the beneficial effects of pericardial matrix derived hydrogel in the context of HL-1 cells.[23] However, these cells are derived from the AT-1 mouse atrial cardiomyocyte tumor lineage, which exhibit ultrastructural characteristics typical of embryonic atrial cardiac muscle cells.[43] Thus, these cells are not clinically relevant. Therefore, we evaluated the behavior of human cells including hMSCs and hiPSC-derived cardiomyocytes on PMCNT-gels. Previously, it has been shown that the beneficial effect of MSCs correlates directly with the number of transplanted MSCs.[44,45] On the other hand, it is difficult to transplant high numbers of MSCs due to low engraftment and survival rate.[18] Therefore, we hypothesized that PMCNT-gels provide a suitable environment to allow hMSC proliferation and expansion upon transplantation. Analyses of alamarBlue™ assays demonstrated that hMSCs proliferate on PMCNT-gels faster than on PM-gels as well as gelatin exhibiting a constant proliferation rate for 168 hours (Fig. S1a†). In order to assess whether hMSCs maintained their multipotency and thus their beneficial paracrine effect, we have analyzed their differentiation potential towards adipose and bone lineages after culturing them for 7 days on PMCNT-gels (Fig. S1b†). Our data show that hMSCs could successfully be differentiated into adipose and bone lineages indicating that hMSCs on the different matrices remained their multipotency.

hiPSCs-derived cardiomyocytes are a promising cell-type for cell-based cardiac therapy. Immunostaining of our hiPSCs revealed the expression of OCT4, SSEA4, TRA-1-60, and SOX2 and therefore their pluripotency (Fig. 3a). Thus, we differentiated these cells into cardiomyocytes using an established protocol utilizing CHIR-99021 and IWR-1-*endo*.[46] Subsequently, we evaluated the viability and beating properties of hiPSC-derived cardiomyocytes. Analyses of viability by live and dead staining showed that after one and seven days, the viability of hiPSC-derived cardiomyocytes on PM- or PMCNT-gels is comparable to cells on Matrigel®, the standard culture substrate for hiPSC-derived cardiomyocytes (Fig. S1c, d† and Fig. 3b, c). Furthermore, Kymograph analyses revealed that hiPSC-derived cardiomyocytes exhibited autonomous contractions on Matrigel®, PM- and PMCNT-gels after seven days (Fig. 3d). However, cells on Matrigel® and PM-gels exhibited arrhythmias (yellow plus signs, Fig. 3d and Movies S1, S2†).

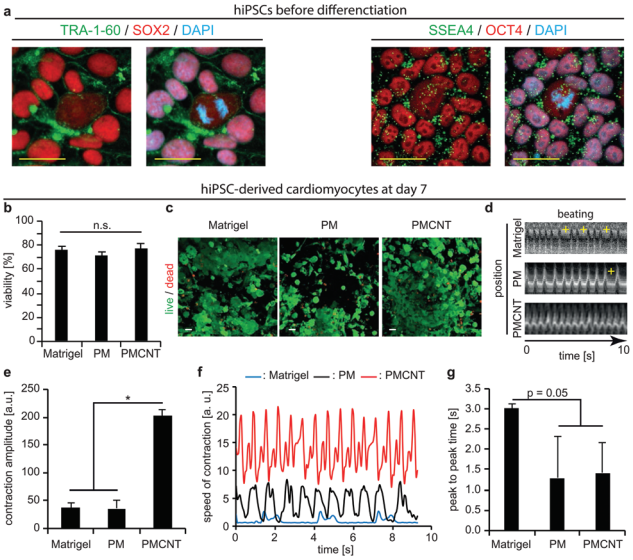

Fig. 3 Analyses of response of the clinically relevant cell types. (a) Examples of projections of confocal images of hiPSCs before differentiation stained for pluripotent markersTRA-1-60, SOX2, SSEA4, OCT4, and DNA (DAPI). (b) Quantitative analysis of live and dead staining (n = 3) based on (c) images of viability of hiPSC-derived cardiomyocytes cultured on 2D films after 7 days based on live and dead staining by calcein-AM (green, living) and ethidium homodimer-1 (EthD-1, red, dead). (d) Examples of Kymograph analysis visualizing autonomous contractions (peaks) of hiPSC-derived cardiomyocytes. Yellow plus signs indicate arrhythmia. (e) MUSCLEMOTION analysis of contraction amplitude (n = 3), (f) examples of speed of contraction at day seven, and (g) peak-to-peak time (n = 3). Data are mean ± SD. *: $p < 0.05$. Scale bars: yellow: 5 μm, white: 10 μm.

Incorporation of carbon nanotubes resulted in synchronous contractions without signs of arrhythmia (Fig. 3d and Movie S3†). In addition, we performed MUSCLEMOTION analyses of the obtained movies at day 7. hiPSC-derived cardiomyocytes grown on PMCNT-gels exhibited significantly greater contraction amplitude (PMCNT: 202.3 ± 11.3 a.u. *vs.* PM: 35.6 ± 15.8 a.u. and Matrigel®: 36.5 ± 9.8 a.u., Fig. 3e). These cells also exhibited a higher speed of contraction on PMCNT-gels (values of normalized speed of contraction of ~14 a.u. *vs.* ~2 a.u. on Matrigel® and ~7.5 a.u. on PM-gels, Fig. 3f). Finally, peak-to-peak time was decreased in cells cultured on both PM- and PMCNT-gels compared to cells on Matrigel® (Fig. 3g). There was a clear trend (p = 0.05), yet, the difference was not significant. Collectively, these data suggest that PMCNT-gels are suitable materials for the expansion of hMSCs as well as culture of hiPSC-derived cardiomyocytes to exhibit rhythmic and efficient contractions.

PMCNT-gels enhance alignment, electrical coupling, and sarcomere maturation

Improved beating properties of engineered cardiac tissues have been shown to be caused by improved cellular alignment, intercellular electrical coupling, and sarcomere maturation which can be induced by mechanical or electrical stimulation of the engineered cardiac tissues[46,47] or intrinsically in electro-

conductive gels.[33] Thus, we have investigated whether hiPSC-derived cardiomyocytes exhibit also on electroconductive PMCNT-gels improved characteristics. Immunostaining images of cardiac troponin I were utilized by Orientation J plugin[48] of NIH ImageJ software in order to quantitatively analyze the orientation distribution of cardiomyocytes on Matrigel®, PM- and PMCNT-gels. Analyses of cellular alignment revealed that the majority of hiPSC-derived cardiomyocytes per observed area exhibit a unidirectional orientation on PMCNT-gels as shown by a narrow orientation distribution (Fig. 4a–c). However, cells on Matrigel® and PM-gels failed to form such orientation, and they showed irregular orientation as measured from immunostaining images and expressed by color-coded (Fig. 4a) as well as radar graphs (Fig. 4b).

In order to determine if intercellular coupling of hiPSC-derived cardiomyocytes is enhanced on PMCNT-gels, cells were stained at day 7 for cardiac-specific markers troponin I and sarcomeric α-actinin as well as the gap junction protein connexin 43 (Fig. 5a). Image analysis revealed that surface coverage of cardiomyocytes based on troponin I staining was not significantly different among all groups (Fig. 5a and b). In contrast, hiPSC-derived cardiomyocytes on PMCNT-gels exhibited a markedly increased expression of connexin 43 indicating improved cell-to-cell contact and coupling (Fig. 5a and c). Finally, PMCNT-gels promoted sarcomere maturation as hiPSC-derived cardiomyocytes exhibited a sarcomeric length of 1.3 ± 0.2 μm on Matrigel®, 1.4 ± 0.2 μm on PM-gels and 1.7 ± 0.3 μm on PMCNT-gels (Fig. 5a and d).

In order to determine if PMCNT-gels are suitable to engineer 3D cardiac tissues, we mixed hiPSC-derived cardiomyocytes with digested ECM and let it gel for 1 h. Immunofluorescence staining analysis revealed that cardiomyocytes elongated and spread through PM- and PMCNT-gels exhibiting a well-established sarcomeric apparatus (Fig. 6a). Analysis of calcium handling *via* Fluo-4 calcium sensitive dyes and live cell imaging indicated that cardiomyocytes in both the PM- and PMCNT-gels showed comparable calcium release and recovery patterns. However, PMCNT-tissues showed slightly higher beating frequencies, greater calcium flux peaks (Fig. 6c and d), and significantly lower time to peak as well as relaxation times (Fig. 6e–g).

We hypothesize that the inclusion of electroconductive materials will be favorable in a clinical point of view as it might help to prevent the issue of arrhythmia. Yet, it remains unclear whether the inclusion of electroconductive materials affects the responsiveness of engineered tissues to external stimuli.

To address this issue, we assessed the response of both PM- and PMCNT-tissues to external electrical stimulation, isoproterenol as well as epinephrine *via* MUSCLEMOTION analysis. Our data demonstrate that the engineered tissues positively

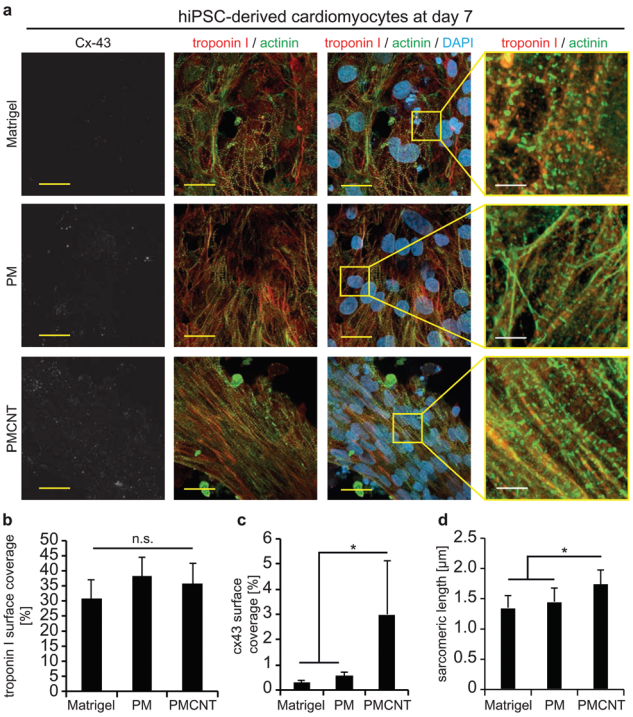

Fig. 5 Conductive biohybrid hydrogels intrinsically enhance intercellular electrical coupling of hiPSC-derived cardiomyocytes. (a) Examples of projections of confocal images of biohybrid hydrogels seeded with hiPSC-derived cardiomyocytes for the cardiomyocyte-specific markers troponin I and/or sarcomeric-α-actinin as well as connexin 43 and DNA (DAPI) at day 7. (b) Quantitative analysis of cardiomyocyte (troponin I) surface coverage (n = 3). (c) Quantitative analysis of connexin 43 surface coverage normalized to troponin I (n = 3). (d) Quantitative analysis of sarcomeric length based on confocal images of hiPSC-derived cardiomyocytes stained for troponin I and sarcomeric-α-actinin in (a) (n = 3). Data are mean ± SD. *: $p < 0.05$. Scale bars: yellow: 10 μm, white: 2 μm.

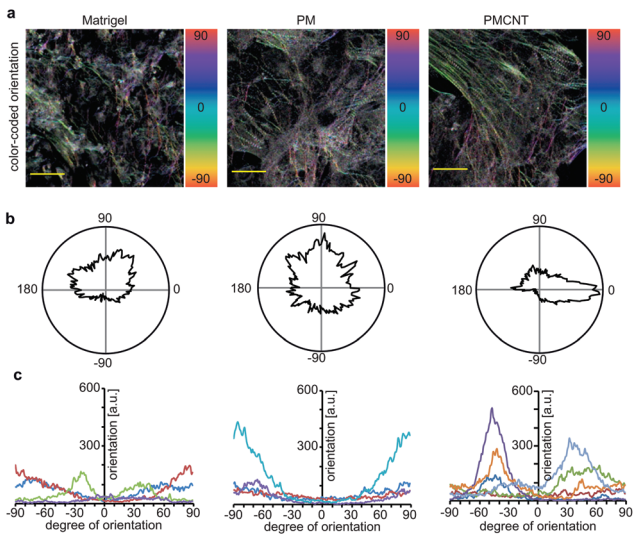

Fig. 4 Conductive biohybrid hydrogels intrinsically enhance alignment and orientation of hiPSC-derived cardiomyocytes. (a) Representative color-coded confocal images of hiPSC-derived cardiomyocytes cultured on hydrogels from utilized troponin I staining in order to determine orientation of cardiomyocytes. (b) Representative radar graphs indicating orientation distribution in an individual image. (c) Orientation distribution of cardiomyocytes in individual images. Scale bars: 10 μm.

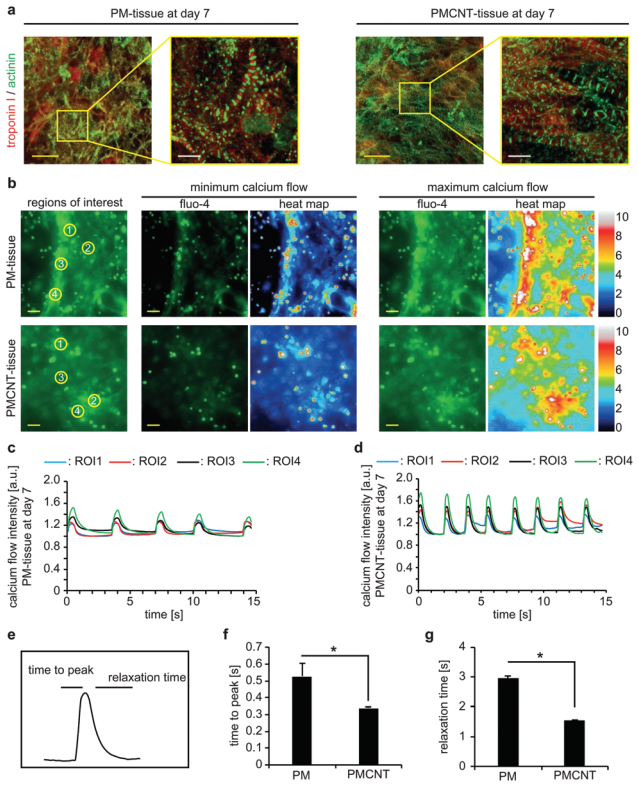

Fig. 6 PMCNT-engineered 3D tissues exhibit enhanced calcium-handling properties. (a) Examples of projections of confocal images of cell-laden tissue constructs stained for the cardiomyocyte-specific markers troponin I and sarcomeric-α-actinin. (b) Local calcium minima and maximum calcium concentration based on Fluo-4 calcium analysis. Analyzed regions of interest (ROI) are indicated by yellow circles. (c, d) Representative examples of intracellular calcium changes of cardiomyocytes in 3D engineered tissues for different ROIs. (e) Schematic illustration of time to peak and relaxation time concept, which has been measured in (f, g) at day 7. Data are mean ± SD. *: $p < 0.05$. Scale bars: yellow: 25 μm, white: 4 μm.

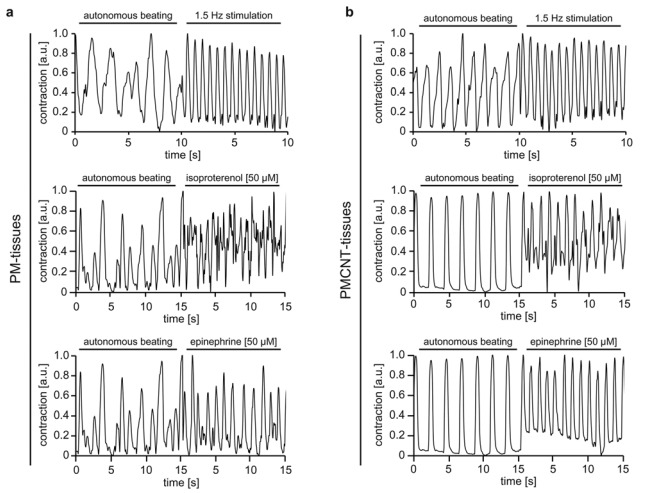

Fig. 7 Engineered cardiac tissues respond to electrical and pharmaceutical stimulations. Examples of contractility of engineered tissues based on MUSCLEMOTION analysis of acquired movies at day 7. (a) PM-tissues and (b) PMCNT-tissues were stimulated by electrical pacing at 1.5 Hz, and exposed to isoproterenol (50 μM) or epinephrine (50 μM).

responded to all these stimuli with increased beating frequencies (Fig. 7a and b). Notably, PMCNT-gels exhibited a more homogenous response than PM-gels (fewer intermediate peaks of lower intensity indicating non-synchronous contractions) (Fig. 7).

In order to evaluate long-term cellular behavior in engineered tissues, we cultured PM- and PMCNT-tissues for 27 days when they still exhibited spontaneous contraction (Movies S6 and S7†). Immunofluorescence staining analysis revealed that cardiomyocytes in both hydrogels formed condensed structures with very well striated sarcomeres (Fig. 8a). Furthermore, engineered tissues responded to drugs that either enhance or inhibit cardiomyocyte contraction (Fig. 8b and c). Stimulation with isoproterenol or epinephrine resulted in an increased beating frequency accompanied by an increased contraction intensity that was higher in PMCNT-tissues compared to PM-tissues. Nifedipine, as an L-type calcium channel blocker, caused a decrease in beating frequency 2 min after treatment and a stop of contraction after 5 min. Verapamil, as a T-type calcium channel blocker, abolished beating of the tissues 2 min post-stimulation. Thus, these tissues can be maintained in culture for long-term and be used as *in vitro* models for cardiac physiology.

In summary, our results suggest that PMCNT-gels without external stimulation can enhance alignment, intercellular electrical coupling, and sarcomere maturation of hiPSC-derived cardiomyocytes resulting in improved beating properties of engineered cardiac tissues. Moreover, engineered PMCNT-tissues exhibited improved calcium handling properties and properly responded to external stimuli.

Discussion

We conclude that PMCNT-gels are promising materials for stem cell-based cardiac tissue engineering to make more opportunities for treating cardiovascular diseases. This conclusion is supported by our findings that PMCNT-gels provide a suitable environment for hMSC proliferation as well as hiPSC-derived cardiomyocyte maturation evidenced by increased connexin 43 expression and increased sarcomere length. Importantly, PMCNT-gel promoted hiPSC-derived cardiomyocyte alignment and increased contractility in the absence of arrhythmia. Moreover, 3D cell-laden PMCNT-engineered tissues exhibited enhanced calcium handling evidenced by shorter time to peak and relaxation time resulting in slightly higher beating frequencies.

Clinical studies based on hMSC therapy for cardiac applications showed beneficial effects, which are due to hMSC-secreted factors. However, cellular engraftment and maintenance post-transplantation is a challenge.[17,18] Thus, one strategy to enhance hMSC-based therapies is to improve hMSC delivery, survival and *in situ* amplification. As the PMCNT-gel

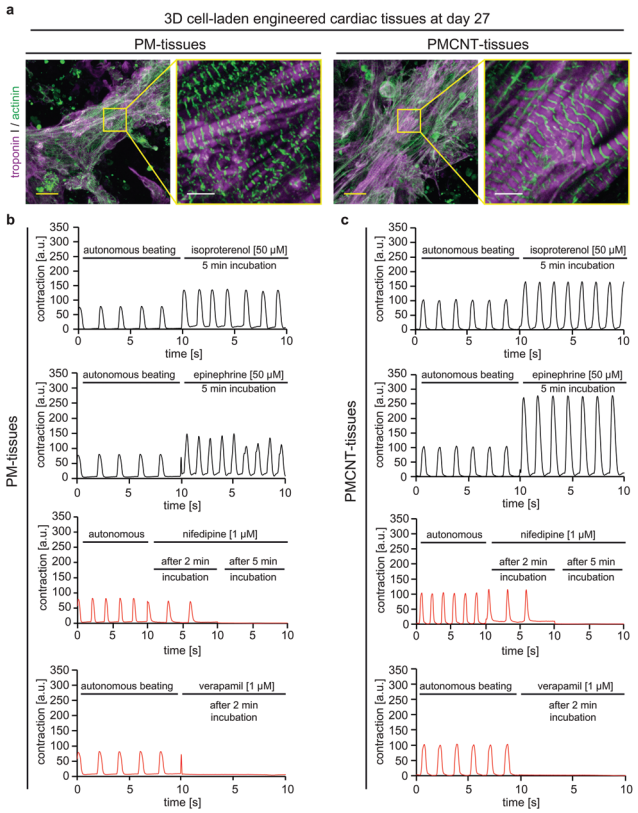

Fig. 8 Engineered cardiac tissues exhibit spontaneous contraction at day 27 and respond to pharmaceutical stimulations. (a) Examples of projections of confocal images of cell-laden tissue constructs stained for the cardiomyocyte-specific markers troponin I and sarcomeric-α-actinin. b, (c) Examples of contractility of engineered tissues based on MUSCLEMOTION analysis of acquired movies. (b) PM-tissues and (c) PMCNT-tissues were stimulated with drugs that enhance (isoproterenol [50 µM], epinephrine [50 µM]) or inhibit (nifedipine [1 µM], verapamil [1 µM]) cardiomyocyte contraction. Scale bars: yellow: 25 µm, white: 5 µm.

provides a suitable microenvironment for proliferation of hMSCs, it is a promising material to be evaluated for enhanced hMSC-based therapies. Furthermore, our data suggest that PMCNT-gels allow the expansion of hMSCs maintaining their multipotency and thus beneficial paracrine effect, as 7 days-long cultured hMSCs could still successfully be differentiated into bone and lipid lineages.

hESC- and hiPSC-derived cardiomyocytes are other promising cell types for regenerating the injured heart. Engraftment of hESC- and hiPSC-derived cardiomyocytes showed promising results.[8,10,13] However, these cells are developmentally immature and therefore they have self-beating characteristics as well as limited force generation capacities.[1] Thus, they are unable to electrically couple with the surrounding cardiac tissue when transplanted. Therefore, transplantation of these cells is often accompanied by cardiac arrhythmia.[8,10] In contrast to Matrigel® and PM-gels, PMCNT-gels promoted rhythmic beating of hiPSC-derived cardiomyocytes and exhibited no toxicity. Furthermore, they generated greater "speed of contraction" as well as "contraction amplitude" on PMCNT-gels. This suggests that hydrazide functionalized carbon nanotubes can provide the biohybrid hydrogel based on pericardial matrix with a suitable environment for rhythmic beating and improved generated force of hiPSC-derived cardiomyocytes.

Force generation of cardiac tissue depends on several factors including cell-to-cell communication, cell alignment and orientation, sarcomeric maturation, as well as mechanical properties of the matrix.[49] Our data show that hiPSC-derived cardiomyocytes on PMCNT-gels expressed higher connexin 43 levels indicating that the cells better couple electrically, as connexin 43 is a protein responsible for electrical coupling of adjacent cells. Moreover, they showed enhanced cellular alignment and contained longer sarcomeres with an average of 1.7 µm. The cause of alignment is unclear, as SEM image of internal structures in PMCNT hydrogel did not show any structural motifs explaining the promotion of cardiomyocyte alignment.

It is well known that electrical stimulation of cardiomyocytes induces cell elongation and alignment as well as centrally positioned elongated nuclei and well-aligned sarcomeres.[46,50] It has been concluded that electrical stimulation enhances cardiomyocyte cross talk by synchronizing their beating as well as facilitating their intercommunication. While external electrical stimulation generates a signal and dominates its propagation, electroconductive biohybrid hydrogels might act as internal enhanced electrical systems that facilitate communication of cardiomyocytes by enhancing the overall conduction. Notably, our observation that electroconductive biohybrid scaffolds induce cellular alignment is not unique. Previously, Ryan AJ *et al.* have shown that electroconductive biohybrid scaffolds made from collagen and graphite promote enhanced alignment without any stimulation.[51] In addition, we have previously described that cardiomyocytes in electroconductive biohybrid hydrogels elongate and align locally while exhibiting enhanced beating characteristics.[33] Based on the in-depth study by Kim Y *et al.* on flexible conductive polymeric systems,[52] we believe that carbon nanotubes act as high aspect ratio conductive fillers in biohybrid hydrogels and generate self-assembled conductive pathways by forming conduction anchor points throughout the gel. These anchor points should facilitate ionic transportation, which is the main conduction mechanism in hydrogels. Cardiomyocytes might recognize these pathways and organize themselves accordingly forming aligned cellular structures. We believe that an electroconductive environment enhances the propagation of the electrical signals, which have been generated by the cells throughout the gel. Thus, these cells can communicate easier and therefore couple better. The improved coupling and beating observed in these cells result in formation of condensed aligned batches of cardiomyocytes that orient themselves unidirectional.

hiPSC-derived cardiomyocytes inside 3D generated cell-laden engineered PMCNT-tissues exhibited enhanced calcium handling properties including shorter time to peak as well as relaxation time. Therefore, hiPSC-derived cardiomyocytes in PMCNT-gels release calcium from their sarcoplasmic reticulum faster as compared to PM-gels resulting in faster contrac-

tion. On the other hand, the shorter relaxation time indicates that the contracted cells regain their initial non-contracted state faster returning to their equilibrium state. Furthermore, we have shown that PMCNT-tissues (7 or 27 days-old) could be used as an *in vitro* model to study effects of external stimuli on cardiac tissue.

Finally, rheometric analyses revealed that PMCNT-gels, probably thanks to the effects of carbon nanotubes, are more elastic (loss tangent: 0.77 for PM-gels *vs.* 0.42 for PMCNT-gels) and thus store and release energy more efficiently. Therefore, this matrix exhibits a lower dampening to cardiomyocyte-generated force. As a comparison, native porcine or bovine myocardium have a loss tangent of ~0.17.[53] Moreover, the addition of MWCNT-CDH increased the storage modulus, indicating stiffness, of PM-gels from 119 ± 51 Pa to 199 ± 48 Pa, which is significantly greater than the storage modulus of decellularized and solubilized human as well as porcine myocardial matrix-derived gels (5.3 ± 0.4 Pa and 6.08 ± 0.38 Pa, respectively[54]). However, it remains lower than the storage modulus of native porcine and bovine myocardium (~20 and 25 kPa, respectively[53]). A possible solution is the maturation of these constructs in a bioreactor utilizing the fact that cardiomyocytes or added non-myocytes (*e.g.* fibroblasts) can produce their own extracellular matrix and thereby increase the overall mechanical properties of the construct. This is one of the reasons why addition of non-myocytes has been proven to benefit cardiac tissue engineering.[7]

Collectively, our data demonstrate that PMCNT-gels improve several parameters known to contribute to efficiently beating and force generating cardiac tissues. While the generated gels do not yet reach the level of native adult human myocardium (*e.g.* sarcomeric length of 2.2 μm), they represent a step forward in enhancing maturation of hiPSCs-derived cardiomyocytes.

Conclusion

We have developed biohybrid conductive PMCNT-hydrogels based on solubilized pericardial matrix and hydrazide functionalized multiwall carbon nanotubes, which elevated the electrical conductivity of the hydrogel. These hydrogels provided a suitable environment for clinically relevant hMSCs as well as hiPSC-derived cardiomyocytes. PMCNT-gels promoted hMSC proliferation, which increases the chances that these cells will also proliferate upon transplantation increasing the number of hMSCs over time and thus enhancing their paracrine effect to promote endogenous cardiac repair. In regards to hiPSC-derived cardiomyocytes, PMCNT-gels exhibited no toxicity and promoted their functionality evidenced by improved calcium handling, contraction amplitude, and speed of contraction as well as the absence of arrhythmia. A detailed analysis revealed that the enhanced functionality results from enhanced cellular alignment and cell-to-cell coupling due to increased connexin 43 expression, as well as increased sarcomeric length and improved mechanical properties of the gel. Overall, we identified PMCNT-gels as promising materials for stem cell-based cardiac tissue engineering to foster hopes for treating cardiovascular diseases. A promising future approach might be the generation of bilayer PMCNT-gels that contain a layer with hiPSC-derived cardiomyocytes to provide immediately additional contractile force as well as a layer with hMSCs to promote endogenous repair mechanisms.

Experimental section

Hydrazide functionalization of nanotubes

Carboxylic acid functionalized multi-walled carbon nanotubes (8% w/v, Sigma 755125) were hydrazide-functionalized using a standard *N*-(3-diethylaminopropyl)-*N*′-ethylcarbodiimide (EDC) coupling as described before[55] with slight modification. Briefly, COOH-MWCNT (100 mg) was dispersed in distilled water (50 mL) by sonication (water bath sonicator, Branson 2510) for 30 min. Carbodihydrazide (Sigma C11006) and hydroxybenzotriazole (Sigma 54802) were dissolved in distilled water (50 mL) separately and added to COOH-MWCNT. Then, pH was adjusted to 4.7 and EDC (Sigma 39391) was added to the solution. The solution was stirred overnight at room temperature and dialyzed through dialysis membranes (Spectra Pro-3, MWCO 3.5 kDa) against diluted HCl (in distilled water, pH = 3) (Fisher Scientific 1330572) and NaCl (0.1 M, Fisher Scientific 1416237) for one day and subsequently against double distilled water for two days. After dialysis, samples were collected and lyophilized (SCANLAF Coolsafe 55-9 De-Ice, LabGene Denmark) for 48–72 hours.

XPS analysis of nanotubes

Elemental evaluation of functionalized MWCNTs was done by using the X-ray photoelectron spectroscopy technique (XPS, Physical Systems Quantum 2000 spectrometer with monochromatic Al Kα radiation) to determine the amount of nitrogen and carbon in carboxylic acid and hydrazide functionalized MWCNTs.

Particle size measurements

Particle size was determined for nanotubes before and after conjugation by dynamic light scattering (DLS) technique. Nanotubes in water were sonicated and their size distribution was assessed less than 15 min after sonication using Zeta Sizer Nano ZS (Malvern Industries Ltd, Malvern, UK). Then, hydrazide functionalized MWCNTs were dispersed in water with different pH-values to investigate the pH-dependent dispersibility of nanotubes. Aliquots of nanotubes (0.1 mg mL^{-1}) were used to measure particle sizes in a volume of 500 μL.

Pericardial matrix preparation

Pericardial tissue was harvested from young adult sheep and immediately transferred to a clean room on dry ice. Excess lipid tissue was dissected and washed several times with deionized water. The pericardium was cut into small pieces, and decellularized as reported.[23] Decellularized pericardial matrix

was lyophilized for 48 h and then cut into fine granular debris and lyophilized again to obtain a powdery, granular pericardial matrix. To confirm decellularization hematoxylin–eosin staining was performed as previously reported.[56] In addition, deoxyribonucleic acid (DNA) was quantified upon staining with 4′,6-diamidino-2-phenylindole dihydrochloride (DAPI). Tissues were fixed in paraformaldehyde (3.7% in Dulbecco's phosphate buffered saline (DPBS), Sigma D8537) and permeabilized in Triton X-100 (2.5% in DPBS) for 15 min; thereafter, samples were incubated with DAPI (5 μg mL^{-1}, Sigma 32670) for 2 min at room temperature (protected from light). Then, fluorescent intensity was measured using a plate reader model Infinite 200 pro Tecan at the excitation/emission of 358/461 nm. sGAG and protein content of the fresh and decellularized tissues were measured based on DBMM assay and PAGE utilizing NuPAGE 4–12% gels followed by Coomassie staining, respectively, as reported previously.[57] Total protein (35 μg) was loaded in each well of the gel and rat tail collagen I (Advanced Biomatrix) at the concentration of 2.5 mg mL^{-1} was used as a control.

Gel preparation

Gels (6 mg mL^{-1}) were prepared following our previous report.[23] Pericardial matrix and pericardial matrix containing nanotubes (0.5%) were prepared by mixing MWCNT-CDH with digested pre-gelled pericardial matrix and subsequent incubation at 37 °C to induce gelation.

Scanning electron microscopy (SEM) analysis

Gels were fixed in paraformaldehyde (3.7% in DPBS) for 1 h, rinsed in a 30, 50, 70, 90, 95 and 100% ethanol series for 30 min each, immersed in ethanol (100%), and critically point dried to preserve the microstructure of the nanofibrous gel (EM CPD300, Leica, 12 cycles, exchange speed of 5 and 120 s delay). Samples were carefully cut into small pieces using a surgical blade, sputter-coated with gold (Q150 T, Quorum technologies Ltd, Germany) and cross-sectional area was analyzed with a Leo 1550 SEM (Zeiss Germany).

Rheometry

Gels were analyzed using a rheometer (AR-2000, TA instruments) as described.[58] A frequency sweep test was done on gels with the diameter of 8 mm and the gap space of 1 mm and 5% strain from 0.5 rad s^{-1} to 100 rad s^{-1} and the storage (G') and loss modulus (G'') were measured.

Swelling ratio

Wet and dry weight of gels were used to calculate swelling ratios as described.[23]

Electrical conductivity measurements

Electrical conductivity was measured at room temperature utilizing a four-point probe device (Loresta AX (MCP-T370) with a MCP-TP06P sensor (N&H technology, Japan)).

Cell culture

Pre-gel solutions were placed in culture vessels. For 2D controls, coverslips were coated with Matrigel® (1 : 160 dilution in DMEM media) for hiPSC-derived cardiomyocytes or with gelatin (0.02 wt% in double distilled water) for hMSCs. hMSCs were cultured at passage number four in the Dulbecco's modified eagle's medium (DMEM) containing FBS (10%) and penicillin/streptomycin (1%). F1 hiPSCs[59] at passage number 24 were cultured and differentiated into cardiomyocytes as previously described.[60] Briefly, hiPSCs (90% confluent) were treated with CHIR-99021 (6 μM) for 2 days. After 1 day of incubation in culture medium without any inhibitor, W_{nt} signaling was inhibited by IWR-1-*endo* (5 μM) for 2 days. Cells were incubated in culture medium for another 2 days. Subsequently, cells were cultured with insulin until day 12. At this stage, cells were considered as 1 day-old cardiomyocytes. RPMI-1640 was used as base medium and B27-minus insulin or B27 were used as supplements.

3D tissue generation

For 3D cell-laden tissues, cardiomyocytes were detached from culture plates using Accutase™ for 8–9 min at 37 °C and subsequently resuspended in pre-gel solution at the density of 4×10^7 cells per mL, were dispensed in 8-well chamber slides (ThermoFisher Scientific), and let it gel for 1 h at 37 °C and 5% CO_2. Then, culture media was added and changed every other day.

hMSC differentiation

Differentiation was achieved by using StemPro™ Adipogenesis and Osteogenesis Differentiation Kits (ThermoFisher Scientific) according to manufacturer's instructions. Differentiated cells were subsequently stained by LipidTox (ThermoFisher Scientific) and Alizarin Red S (ThermoFisher Scientific) staining for detection of adipose and bone lineages, respectively. In order to better visualize Alizarin Red staining, NIH Image J software was utilized to provide look up table (LUT) color-coded images with enhanced contrast.

Cellular proliferation and viability

The proliferation of cells was measured by the Alamar blue assay as reported.[23] Alamar blue dye (Fisher Scientific 10099022) was diluted in culture medium to 10%, added to the cells and subsequently the cells were incubated for 2 h at 37 °C and 5% CO_2. Then, samples were analyzed at 560/590 nm using plate reader model Infinite 200 pro-Tecan at gain 80. In addition, viability of cells was determined using Live and dead assay kit (L3224, Invitrogen)[61] and images were quantified using NIH ImageJ software.

Immunostaining

Samples were fixed in paraformaldehyde (3.7% in DPBS) for 30 min, permeabilized in Triton X-100 (0.25% in DPBS) for 20 min and immunostained for cardiac-specific markers as previously described.[61] The following primary antibodies were utilized: mouse anti-sarcomeric α-actinin (1 : 250, Abcam,

ab9465), rabbit anti-connexin 43 (1 : 50, Santa Cruz Biotechnologies, sc-9059), goat anti-cardiac troponin I (1 : 250, Abcam, ab56357). Pluripotency was assessed after 15 min fixation, 15 min permeabilizing, and 30 min blocking (BSA, 5 wt/v %), Tween20 (0.2 v/v % in PBS) with the following antibodies: mouse anti-human TRA-1-60 (MA-1-023), rat anti-human SOX2 (14-9811-82) (both 1 : 100), mouse anti-human SSEA4 (MA1-021), rabbit anti-human Oct4 (MA5-1484) (both 1 : 250) (all Thermofisher). Secondary antibodies conjugated with ALEXA 488-, ALEXA 594- or ALEXA 647 were used for fluorescent detection (2 h incubation, 1 : 500; Molecular Probes). DNA was visualized with DAPI (0.5 g ml^{-1} in 0.1 wt/v % NP40, 7 min).

Calcium handling properties

Fluo-4 Direct™ Calcium Assay Kit (ThermoFisher Scientific) was used to analyze calcium handling properties of 3D cell-laden engineered tissues using PM- and PMCNT-gels following the manufacture's instructions. The fluorescent movies were acquired using a live cell imaging setup (Keyence Microscopy).

Electrical stimulation

PM- and PMCNT-tissues cultured for 7 days were stimulated with a homemade four point-based electrical pacer at 1.5 Hz.

Pharmaceutical stimulation

PM- and PMCNT-tissues were cultured for 7 days and then exposed to isoproterenol (50 μM) or epinephrine (50 μM) or for 27 days and exposed to isoproterenol (50 μM), epinephrine (50 μM), nifedipine (1 μM), or verapamil (1 μM).

Movie acquisition

Movies of 2D cultures were recorded in wells of 6-well plates for 10 to 15 s. For calcium handling assays, movies were recorded for 10 s utilizing 24-well plates. Movies of electrical stimulated cardiac tissues were recorded in ∅ 35 mm Petri dishes for 10 s before and 10 s after pacing. As drug stimulation was not compatible with the microscope set up, cardiac tissues were recorded in 8-well chamber slides for 15 s at day 7 or 10 s at day 27, then, tissues were stimulated and incubated for 5 min at day 7 or 2 min and 5 min at day 27 at 37 °C and 5% CO_2, and subsequently recorded for another 15 s. All movies were recorded under a Keyence BZ9000 microscope.

Beating characteristics

Movies were analyzed by Kymograph[61] as well as MUSCLEMOTION[62] plugin for NIH image J.

Orientation distribution analysis

Orientation J[48] plugin for NIH ImageJ software was used in order to measure cellular orientation distribution and generating color-coded images based on cardiac troponin I immunostaining images of hiPSC-derived cardiomyocytes.

Statistical analyzes

Data of at least three independent experiments are expressed as mean ± SD. Statistical significance of differences was evaluated by a two-tailed Student's *t*-test (Excel) or where appropriate by one way analysis of variance (ANOVA) followed by Bonferroni's *post hoc* test (IBM SPSS). $p < 0.05$ was considered statistically significant.

Ethical statement

All animal procedures were performed in accordance with the Guidelines for Care and Use of Laboratory Animals of the Friedrich-Alexander-Universität Erlangen-Nürnberg and approved by the Animal Ethics Committee of the government of Unterfranken, Germany (Az. 54-2532.1-44/11 of the government of Mittelfranken, Germany and AZ 55.2-2532-2-465 of the government of Unterfranken, Germany). The investigation conforms with the guidelines from Directive 2010/63/EU of the European Parliament on the protection of animals used for scientific purposes.

Conflicts of interest

There are no conflicts to declare.

Acknowledgements

Authors would like to thank Marina Leone for her help on the analysis of protein content of the matrix (PAGE analysis, Coomassie staining), Tilman Esser for his support with the cell culture, Tilmann Volk and Stephan Achenbach for cardiac inhibitory drugs (nifedipine and verapamil), and Annika Weigand for providing sheep pericardial tissue. This work was funded by the Deutsche Forschungsgemeinschaft (DFG, German Research Foundation) – Projektnummer 326998133 – TRR 225 (subproject C01 to F. B. E.) and individual grants (EN 453/11-1 and INST 410/91-1 FUGG both to F. B. E.), as well as the Universitätsbund Erlangen-Nürnberg e.V. (to F. B. E.).

Notes and references

1 T. Eschenhagen, R. Bolli, T. Braun, L. J. Field, B. K. Fleischmann, J. Frisen, M. Giacca, J. M. Hare, S. Houser, R. T. Lee, E. Marban, J. F. Martin, J. D. Molkentin, C. E. Murry, P. R. Riley, P. Ruiz-Lozano, H. A. Sadek, M. A. Sussman and J. A. Hill, *Circulation*, 2017, **136**, 680–686.

2 E. J. Benjamin, S. S. Virani, C. W. Callaway, A. M. Chamberlain, A. R. Chang, S. Cheng, S. E. Chiuve, M. Cushman, F. N. Delling, R. Deo, S. D. de Ferranti, J. F. Ferguson, M. Fornage, C. Gillespie, C. R. Isasi, M. C. Jimenez, L. C. Jordan, S. E. Judd, D. Lackland, J. H. Lichtman, L. Lisabeth, S. Liu, C. T. Longenecker, P. L. Lutsey, J. S. Mackey, D. B. Matchar, K. Matsushita, M. E. Mussolino, K. Nasir, M. O'Flaherty, L. P. Palaniappan, A. Pandey, D. K. Pandey, M. J. Reeves,

M. D. Ritchey, C. J. Rodriguez, G. A. Roth, W. D. Rosamond, U. K. A. Sampson, G. M. Satou, S. H. Shah, N. L. Spartano, D. L. Tirschwell, C. W. Tsao, J. H. Voeks, J. Z. Willey, J. T. Wilkins, J. H. Wu, H. M. Alger, S. S. Wong, P. Muntner and E. American Heart Association Council on, C. Prevention Statistics and S. Stroke Statistics, *Circulation*, 2018, **137**, e67–e492.

3 G. L. Wells, *Curr. Vasc. Pharmacol.*, 2016, **14**, 452–457.

4 D. S. Jones and J. A. Greene, *Am. J. Public Health*, 2013, **103**, 1207–1218.

5 O. Jawoniyi, K. Gormley, E. McGleenan and H. R. Noble, *J. Clin. Nurs.*, 2018, **27**, e726–e738.

6 M. M. Kittleson, *F1000Research*, 2018, **7**, 1008.

7 B. M. Ogle, N. Bursac, I. Domian, N. F. Huang, P. Menasche, C. E. Murry, B. Pruitt, M. Radisic, J. C. Wu, S. M. Wu, J. Zhang, W. H. Zimmermann and G. Vunjak-Novakovic, *Sci. Transl. Med.*, 2016, **8**, 342ps313.

8 J. J. Chong, X. Yang, C. W. Don, E. Minami, Y. W. Liu, J. J. Weyers, W. M. Mahoney, B. Van Biber, S. M. Cook, N. J. Palpant, J. A. Gantz, J. A. Fugate, V. Muskheli, G. M. Gough, K. W. Vogel, C. A. Astley, C. E. Hotchkiss, A. Baldessari, L. Pabon, H. Reinecke, E. A. Gill, V. Nelson, H. P. Kiem, M. A. Laflamme and C. E. Murry, *Nature*, 2014, **510**, 273–277.

9 Y. Shiba, S. Fernandes, W. Z. Zhu, D. Filice, V. Muskheli, J. Kim, N. J. Palpant, J. Gantz, K. W. Moyes, H. Reinecke, B. Van Biber, T. Dardas, J. L. Mignone, A. Izawa, R. Hanna, M. Viswanathan, J. D. Gold, M. I. Kotlikoff, N. Sarvazyan, M. W. Kay, C. E. Murry and M. A. Laflamme, *Nature*, 2012, **489**, 322–325.

10 Y. W. Liu, B. Chen, X. Yang, J. A. Fugate, F. A. Kalucki, A. Futakuchi-Tsuchida, L. Couture, K. W. Vogel, C. A. Astley, A. Baldessari, J. Ogle, C. W. Don, Z. L. Steinberg, S. P. Seslar, S. A. Tuck, H. Tsuchida, A. V. Naumova, S. K. Dupras, M. S. Lyu, J. Lee, D. W. Hailey, H. Reinecke, L. Pabon, B. H. Fryer, W. R. MacLellan, R. S. Thies and C. E. Murry, *Nat. Biotechnol.*, 2018, **36**, 597–605.

11 R. Rikhtegar, M. Pezeshkian, S. Dolati, N. Safaie, A. Afrasiabi Rad, M. Mahdipour, M. Nouri, A. R. Jodati and M. Yousefi, *Biomed. Pharmacother.*, 2018, **109**, 304–313.

12 P. Menasche and V. Vanneaux, *Curr. Res. Transl. Med.*, 2016, **64**, 97–106.

13 D. Cyranoski, *Nature*, 2018, **557**, 619–620.

14 E. A. Mol, M. J. Goumans and J. P. G. Sluijter, *Adv. Exp. Med. Biol.*, 2017, **998**, 207–219.

15 F. J. Vizoso, N. Eiro, S. Cid, J. Schneider and R. Perez-Fernandez, *Int. J. Mol. Sci.*, 2017, **18**, 1852.

16 J. P. G. Sluijter, S. M. Davidson, C. M. Boulanger, E. I. Buzas, D. P. V. de Kleijn, F. B. Engel, Z. Giricz, D. J. Hausenloy, R. Kishore, S. Lecour, J. Leor, R. Madonna, C. Perrino, F. Prunier, S. Sahoo, R. M. Schiffelers, R. Schulz, L. W. Van Laake, K. Ytrehus and P. Ferdinandy, *Cardiovasc. Res.*, 2018, **114**, 19–34.

17 D. A. M. Feyen, R. Gaetani, P. A. Doevendans and J. P. G. Sluijter, *Adv. Drug Delivery Rev.*, 2016, **106**, 104–115.

18 R. Madonna, L. W. Van Laake, S. M. Davidson, F. B. Engel, D. J. Hausenloy, S. Lecour, J. Leor, C. Perrino, R. Schulz, K. Ytrehus, U. Landmesser, C. L. Mummery, S. Janssens, J. Willerson, T. Eschenhagen, P. Ferdinandy and J. P. Sluijter, *Eur. Heart J.*, 2016, **37**, 1789–1798.

19 D. A. Pijnappels, S. Gregoire and S. M. Wu, *Ann. N. Y. Acad. Sci.*, 2010, **1188**, 7–14.

20 K. Zhu, S. R. Shin, T. van Kempen, Y. C. Li, V. Ponraj, A. Nasajpour, S. Mandla, N. Hu, X. Liu, J. Leijten, Y. D. Lin, M. A. Hussain, Y. S. Zhang, A. Tamayol and A. Khademhosseini, *Adv. Funct. Mater.*, 2017, **27**, 1605352.

21 A. Navaei, H. Saini, W. Christenson, R. T. Sullivan, R. Ros and M. Nikkhah, *Acta Biomater.*, 2016, **41**, 133–146.

22 A. Wickham, M. Vagin, H. Khalaf, S. Bertazzo, P. Hodder, S. Danmark, T. Bengtsson, J. Altimiras and D. Aili, *Nanoscale*, 2016, **8**, 14146–14155.

23 K. Roshanbinfar, J. Hilborn, O. P. Varghese and O. P. Oommen, *RSC Adv.*, 2017, **7**, 31980–31988.

24 S. R. Shin, B. Aghaei-Ghareh-Bolagh, X. G. Gao, M. Nikkhah, S. M. Jung, A. Dolatshahi-Pirouz, S. B. Kim, S. M. Kim, M. R. Dokmeci, X. W. Tang and A. Khademhosseini, *Adv. Funct. Mater.*, 2014, **24**, 6136–6144.

25 L. M. Amirabad, M. Massumi, M. Shamsara, I. Shabani, A. Amari, M. M. Mohammadi, S. Hosseinzadeh, S. Vakilian, S. K. Steinbach, M. R. Khorramizadeh, M. Soleimani and J. Barzin, *ACS Appl. Mater. Interfaces*, 2017, **9**, 6849–6864.

26 D. Kai, M. P. Prabhakaran, G. R. Jin and S. Ramakrishna, *J. Biomed. Mater. Res., Part A*, 2011, **99**, 376–385.

27 C. W. Hsiao, M. Y. Bai, Y. Chang, M. F. Chung, T. Y. Lee, C. T. Wu, B. Maiti, Z. X. Liao, R. K. Li and H. W. Sung, *Biomaterials*, 2013, **34**, 1063–1072.

28 M. Nishizawa, H. Nozaki, H. Kaji, T. Kitazume, N. Kobayashi, T. Ishibashi and T. Abe, *Biomaterials*, 2007, **28**, 1480–1485.

29 L. Y. Wang, J. Z. Jiang, W. X. Hua, A. Darabi, X. P. Song, C. Song, W. Zhong, M. M. Q. Xing and X. Z. Qiu, *Adv. Funct. Mater.*, 2016, **26**, 4293–4305.

30 J. O. You, M. Rafat, G. J. Ye and D. T. Auguste, *Nano Lett.*, 2011, **11**, 3643–3648.

31 N. Gospodinova and L. Terlemezyan, *Prog. Polym. Sci.*, 1998, **23**, 1443–1484.

32 L. Wang, Y. Wu, T. Hu, B. Guo and P. X. Ma, *Acta Biomater.*, 2017, **59**, 68–81.

33 K. Roshanbinfar, L. Vogt, B. Greber, S. Diecke, A. R. Boccaccini, T. Scheibel and F. B. Engel, *Adv. Funct. Mater.*, 2018, 1803951.

34 C. L. Johnson, E. Snoeck, M. Ezcurdia, B. Rodriguez-Gonzalez, I. Pastoriza-Santos, L. M. Liz-Marzan and M. J. Hytch, *Nat. Mater.*, 2008, **7**, 120–124.

35 J. Hilding, E. A. Grulke, Z. G. Zhang and F. Lockwood, *J. Dispersion Sci. Technol.*, 2003, **24**, 1–41.

36 M. Montgomery, S. Ahadian, L. Davenport Huyer, M. Lo Rito, R. A. Civitarese, R. D. Vanderlaan, J. Wu, L. A. Reis, A. Momen, S. Akbari, A. Pahnke, R. K. Li, C. A. Caldarone and M. Radisic, *Nat. Mater.*, 2017, **16**, 1038–1046.

37 A. A. Rane and K. L. Christman, *J. Am. Coll. Cardiol.*, 2011, **58**, 2615–2629.
38 R. M. Wang and K. L. Christman, *Adv. Drug Delivery Rev.*, 2016, **96**, 77–82.
39 M. T. Spang and K. L. Christman, *Acta Biomater.*, 2018, **68**, 1–14.
40 M. Kharaziha, S. R. Shin, M. Nikkhah, S. N. Topkaya, N. Masoumi, N. Annabi, M. R. Dokmeci and A. Khademhosseini, *Biomaterials*, 2014, **35**, 7346–7354.
41 V. Martinelli, G. Cellot, F. M. Toma, C. S. Long, J. H. Caldwell, L. Zentilin, M. Giacca, A. Turco, M. Prato, L. Ballerini and L. Mestroni, *Nano Lett.*, 2012, **12**, 1831–1838.
42 S. R. Shin, S. M. Jung, M. Zalabany, K. Kim, P. Zorlutuna, S. B. Kim, M. Nikkhah, M. Khabiry, M. Azize, J. Kong, K. T. Wan, T. Palacios, M. R. Dokmeci, H. Bae, X. S. Tang and A. Khademhosseini, *ACS Nano*, 2013, **7**, 2369–2380.
43 W. C. Claycomb, N. A. Lanson Jr., B. S. Stallworth, D. B. Egeland, J. B. Delcarpio, A. Bahinski and N. J. Izzo Jr., *Proc. Natl. Acad. Sci. U. S. A.*, 1998, **95**, 2979–2984.
44 M. Wysoczynski, A. Khan and R. Bolli, *Circ. Res.*, 2018, **123**, 138–158.
45 R. Madonna, P. Ferdinandy, R. De Caterina, J. T. Willerson and A. J. Marian, *Circ. Res.*, 2014, **115**, e71–e78.
46 K. Ronaldson-Bouchard, S. P. Ma, K. Yeager, T. Chen, L. Song, D. Sirabella, K. Morikawa, D. Teles, M. Yazawa and G. Vunjak-Novakovic, *Nature*, 2018, **556**, 239–243.
47 M. N. Hirt, J. Boeddinghaus, A. Mitchell, S. Schaaf, C. Bornchen, C. Muller, H. Schulz, N. Hubner, J. Stenzig, A. Stoehr, C. Neuber, A. Eder, P. K. Luther, A. Hansen and T. Eschenhagen, *J. Mol. Cell. Cardiol.*, 2014, **74**, 151–161.
48 F. Xu, T. Beyazoglu, E. Hefner, U. A. Gurkan and U. Demirci, *Tissue Eng., Part C*, 2011, **17**, 641–649.
49 N. T. Feric and M. Radisic, *Adv. Drug Delivery Rev.*, 2016, **96**, 110–134.
50 M. Radisic, H. Park, H. Shing, T. Consi, F. J. Schoen, R. Langer, L. E. Freed and G. Vunjak-Novakovic, *Proc. Natl. Acad. Sci. U. S. A.*, 2004, **101**, 18129–18134.
51 A. J. Ryan, C. J. Kearney, N. Shen, U. Khan, A. G. Kelly, C. Probst, E. Brauchle, S. Biccai, C. D. Garciarena, V. Vega-Mayoral, P. Loskill, S. W. Kerrigan, D. J. Kelly, K. Schenke-Layland, J. N. Coleman and F. J. O'Brien, *Adv. Mater.*, 2018, **30**, e1706442.
52 Y. Kim, J. Zhu, B. Yeom, M. Di Prima, X. Su, J. G. Kim, S. J. Yoo, C. Uher and N. A. Kotov, *Nature*, 2013, **500**, 59–63.
53 S. Ramadan, N. Paul and H. E. Naguib, *Biomed. Mater.*, 2017, **12**, 025013.
54 T. D. Johnson, J. A. Dequach, R. Gaetani, J. Ungerleider, D. Elhag, V. Nigam, A. Behfar and K. L. Christman, *Biomater. Sci.*, 2014, **2014**, 60283D.
55 S. P. Hudson, R. Langer, G. R. Fink and D. S. Kohane, *Biomaterials*, 2010, **31**, 8.
56 J. L. Ungerleider, T. D. Johnson, N. Rao and K. L. Christman, *Methods*, 2015, **84**, 7.
57 J. L. Ungerleider, T. D. Johnson, N. Rao and K. L. Christman, *Methods*, 2015, **84**, 53–59.
58 S. B. S. M. Seif-Naraghi, P. J. Schup-Magoffin, D. P. Hu and L. Christman Karen, *Tissue Eng., Part A*, 2010, **16**, 11.
59 M. Marczenke, I. Piccini, I. Mengarelli, J. Fell, A. Ropke, G. Seebohm, A. O. Verkerk and B. Greber, *Front. Physiol.*, 2017, **8**, 469.
60 A. Sharma, C. Marceau, R. Hamaguchi, P. W. Burridge, K. Rajarajan, J. M. Churko, H. Wu, K. I. Sallam, E. Matsa, A. C. Sturzu, Y. Che, A. Ebert, S. Diecke, P. Liang, K. Red-Horse, J. E. Carette, S. M. Wu and J. C. Wu, *Circ. Res.*, 2014, **115**, 556–566.
61 J. Petzold, T. B. Aigner, F. Touska, K. Zimmermann, T. Scheibel and F. B. Engel, *Adv. Funct. Mater.*, 2017, **27**, 1701427.
62 L. Sala, B. J. van Meer, L. G. J. Tertoolen, J. Bakkers, M. Bellin, R. P. Davis, C. Denning, M. A. E. Dieben, T. Eschenhagen, E. Giacomelli, C. Grandela, A. Hansen, E. R. Holman, M. R. M. Jongbloed, S. M. Kamel, C. D. Koopman, Q. Lachaud, I. Mannhardt, M. P. H. Mol, D. Mosqueira, V. V. Orlova, R. Passier, M. C. Ribeiro, U. Saleem, G. L. Smith, F. L. Burton and C. L. Mummery, *Circ. Res.*, 2018, **122**, e5–e16.